NANO LETTERS

Letter

pubs.acs.org/NanoLett

Graphene Near-Degenerate Four-Wave Mixing for Phase Characterization of Broadband Pulses in Ultrafast Microscopy

Richard Ciesielski,[†] Alberto Comin,[†] Matthias Handloser,[†] Kevin Donkers,[†] Giovanni Piredda,[‡] Antonio Lombardo,[§] Andrea C. Ferrari,[§] and Achim Hartschuh*,[†]

[†]Department Chemie and CeNS, Ludwig Maximilians Universität München, Butenandtstrasse 5-13, 81377 Munich, Germany

[‡]Josef Ressel Zentrum, Fachhochschule Vorarlberg, Hochschulstrasse 1, 6850 Dornbirn, Austria

[§]Cambridge Graphene Centre, University of Cambridge, 9 JJ Thomson Avenue, Cambridge CB3 0FA, United Kingdom

Supporting Information

ABSTRACT: We investigate near-degenerate four-wave mixing in graphene using femtosecond laser pulse shaping microscopy. Intense near-degenerate four-wave mixing signals on either side of the exciting laser spectrum are controlled by amplitude and phase shaping. Quantitative signal modeling for the input pulse parameters shows a spectrally flat phase response of the near-degenerate four-wave mixing due to the linear dispersion of the massless Dirac Fermions in graphene. Exploiting these properties we demonstrate that graphene is uniquely suited for the intrafocus phase characterization and compression of broadband laser pulses, circumventing disadvantages of common methods utilizing second or third harmonic light.

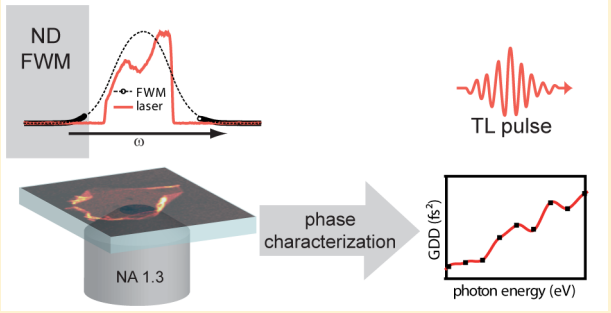

KEYWORDS: *Graphene, four-wave mixing, pulse shaping, femtosecond laser, microscopy, phase retrieval*

The linear dispersion of the massless Dirac Fermions in graphene is enabling an ever increasing number of optical and optoelectronic applications.[1−4] The resulting spectrally flat absorption in combination with ultrahigh electric switching rates make graphene particularly interesting for high-speed applications in photodetectors[3,5,6] and as broadband saturable absorbers in ultrafast lasers.[2,7] The linear dispersion is also connected to efficient higher-order optical responses, including nonlinear broadband photoluminescence and four-wave mixing (FWM).[8−11]

Nondegenerate FWM at $\omega_{FWM} = 2\omega_1 - \omega_2$ in graphene was theoretically described in refs 9 and 12 and experimentally demonstrated in ref 10. The large nonlinearity of graphene, as shown by a $\chi^{(3)}$, which is 2 orders of magnitude higher than the nonlinearities observed for comparable gold films,[13] is explained by the fact that all vertical transitions are resonant at all frequencies ω_{FWM}, ω_1 and ω_2.[10]

Reference 12 theoretically showed that the FWM response is dispersionless with respect to the phase and its intensity is spectrally smooth, scaling as ω^{-4}. FWM from graphene has been use, or proposed, for various applications, such as wavelength conversion in all-fiber configurations,[14,15] in vitro imaging in biological samples,[16] and phase matching for perfect lens applications.[17,18]

A major challenge in ultrafast microscopy is the dispersion of the optical components and the resulting temporal broadening of laser pulses. This can become a significant problem in the case of high-numerical aperture microscope objectives and other elements, such as lenses, windows and dielectric filters.[19] Common procedures for intrafocus pulse compression include frequency resolved optical gating (FROG)[20] and multiphoton intrapulse interference phase scans (MIIPS).[21−23] These rely on the second harmonic generation from reference materials, for example, beta barium borate or iron(III) iodate crystals.[24] These procedures thus require optical components suitable for both fundamental and harmonic frequencies. For broadband laser pulses centered from the visible to the near-infrared, this would require microscope objectives, immersion liquids, substrates, and lenses, as well as sensitive detectors that are also suitable for the ultraviolett, which are in many cases not available. In particular for epi-detection using the same microscope objective for focusing and collection this is a major difficulty with respect to spectral transmittance and chromatic aberrations.

Here, we propose to use the near-degenerate four-wave mixing signal of graphene as a nonlinear optical signal to determine the spectral phase profile of laser pulses in the focus of microscope objectives. Because near-degenerate FWM occurs at energies similar to the excitation, and given the flat spectral response of graphene, this procedure would also be applicable to broadband laser pulses with a temporal duration below 50 fs. We find that the emission spectrum of graphene

Received: March 6, 2015
Revised: June 8, 2015
Published: June 29, 2015

DOI: 10.1021/acs.nanolett.5b00893
Nano Lett. 2015, 15, 4968−4972

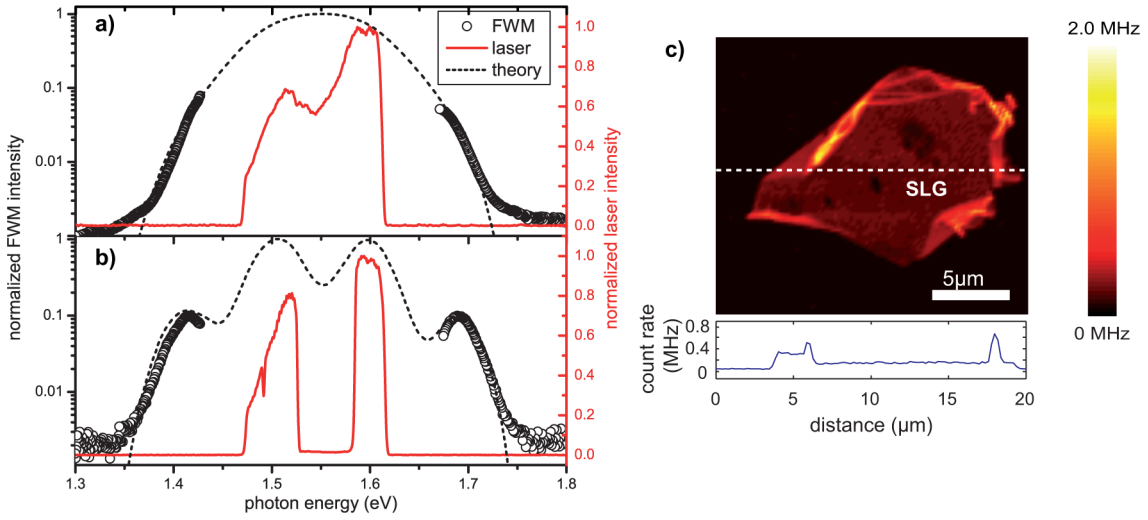

Figure 1. (a) ND-FWM spectrum of single layer graphene (SLG) on glass (semilog plot). The laser pulse is transform limited in the focus of the objective and has a full width at half-maximum of 15 fs. The dashed line corresponds to the calculated FWM-spectrum on the basis of a flat spectral amplitude and phase response and the spectrum of the incident laser. (b) The ND-FWM signal originating from a tailored excitation spectrum follows the theoretical prediction. (c) Confocal scan (Stokes side) of SLG on glass. ND-FWM provides a nearly background free signal contrast that highlights features such as wrinkles. The dashed line indicates the position of the cross section.

close to the energy of an ultrafast laser pulse is dominated by very intense near-degenerate FWM (ND-FWM). We then show that the spectral phase response of $\chi^{(3)}$ in the range 1.47−1.62 eV is flat, implying a dispersionless and instantaneous parametric process for the 15 fs pulses used in our experiments. The nonlinear response of graphene is therefore very well suited for phase characterization. We finally demonstrate the compression of a 15 fs laser pulse in the focus of an objective with a numerical aperture (NA) of 1.3.

We study micromechanically exfoliated single layer graphene (SLG) deposited on glass, using confocal scanning microscopy. An oil-immersion objective (NA = 1.3) is used to excite the sample and to collect the backscattered light. The laser source is a Titanium-Sapphire oscillator, producing trains of 15 fs pulses at a repetition rate of 80 MHz. The central photon energy is 1.55 eV (800 nm) and the bandwidth 0.2 eV (100 nm). We estimate the laser fluence in the focus from the pulse energy of 5.4 pJ, and the diameter of the diffraction limited focal spot $d = 0.61\ \lambda/\mathrm{NA} = 375$ nm to be 49 J/m^2. A pulse-shaper in 4f configuration is used both for compensating the optical dispersion introduced by the setup and for providing additional phase and amplitude modulation. Details of sample preparation and setup are in the Supporting Information.

Figure 1a plots the single layer graphene emission spectrum excited by a 15 fs laser pulse centered at 1.55 eV in the focus of a high NA = 1.3 objective. On both sides of the excitation pulse an intense signal is seen, decaying rapidly with increasing energy shift. In the following, we verify that this signal indeed results from near degenerate four-wave mixing, which is maximized for the shortest (bandwidth limited) pulse.

As a parametric process, four-wave mixing has several realizations fulfilling energy conservation:[25] $\omega_{\mathrm{FWM}} = |\pm\omega_1 \pm \omega_2 \pm \omega_3|$. Typically one can distinguish a degenerate and a near-degenerate case, where $\omega_{\mathrm{FWM}}^{\mathrm{degenerate}}$ equals one of the three input frequencies and $\omega_{\mathrm{FWM}}^{\mathrm{non\text{-}degenerate}}$ is different from all of them.[10,25] In the case of a broadband laser, frequency mixing terms across the spectrum become important and lead to significant contributions directly next to the laser spectrum, defining the near degenerate case.[25,26]

Four-wave mixing spectra can be calculated according to the following integral:[25]

$$I(\omega) = c\varepsilon_0|\chi^{(3)}\int_{\omega_{\min}}^{\omega_{\max}} \mathrm{d}\Omega_1 \int_{\omega_{\min}}^{\omega_{\max}} \mathrm{d}\Omega_2 E(\Omega_1)E(\Omega_2) \times E(\Omega_1 + \Omega_2 - \omega)e^{i[\varphi(\Omega_1)+\varphi(\Omega_2)-\varphi(\Omega_1+\Omega_2-\omega)]}|^2 \quad (1)$$

where E is the amplitude of the excitation laser field, c is the speed of light, ε_0 is the vacuum permittivity, $\omega_{\min}$ and $\omega_{\max}$ are the lower and upper frequency limits of the laser spectrum, and $\varphi(\omega)$ is the spectral phase of the pulse. We determine the total emitted four-wave mixing energy per incoming pulse in two steps. First, we scale the calculated FWM spectrum (dashed line in Figure 1a) to the measured intensity taking into account the overall detection sensitivity of the setup. This allows to access the FWM intensity also in the nonmeasurable regime covered by the laser pulse. Integrating the scaled spectrum we obtain the full FWM energy per pulse of 10^{-17} J, corresponding to the spectral integral over eq 1. From this, we determine a value of $\chi^{(3)} = 4.3 \times 10^{-6}$ esu for the nonlinear susceptibility at a central energy of 1.55 eV. This result is in general agreement with the value of $\chi^{(3)} = 1.5 \times 10^{-7}$ esu reported in ref 10, while the deviation could result from the tight focusing of the excitation pulse in the present measurement, in combination with the nonlinearity of the signal.[27]

According to refs 9 and 10, $\chi^{(3)}$ in single layer graphene is inversely proportional to the fourth power of the frequency ($\chi^{(3)} \propto \omega^{-4}$), but exhibits no phase dependence. Within the 100 nm spectral bandwidth of our laser pulse, this fourth order dependence results in a variation of 40%, at most. Remarkably, the influence of this scaling factor on the emitted intensity is only minor (see Figure S6 of the Supporting Information). This is due to the spectral integration and the mixing of the frequency components seen in Figure 1, which leads to a broad and structureless emission spectrum.

Newer theoretical results[28] also suggest a general phase dependence of the third order nonlinearity in graphene, but this is negligible in the range studied in this work (see Figure S7 in

DOI: 10.1021/acs.nanolett.5b00893
Nano Lett. 2015, 15, 4968−4972

the Supporting Information for details). We thus calculate the ND-FWM spectra using a constant third order susceptibility $\chi^{(3)}$ and the measured laser spectrum (dashed line in Figure 1a,b). This is in good agreement with the experimental response, as seen in Figure 1a,b. At energies further away from the excitation, the experimental signal exceeds the theoretical curve, which we attribute to nonlinear photoluminescence.[8,29,30] This contribution is at least 2 orders of magnitude lower than the four-wave mixing signal. Furthermore, the power dependence is cubic for ND-FWM,[25] while it is roughly quadratic for nonlinear photoluminescence,[29] providing another means to distinguish the two contributions.

The case of two spectrally separated excitation pulses $E_1(\omega)$ and $E_2(\omega)$ is implemented in Figure 1b. Here intrapulse frequency mixing within E_1 and E_2 does not contribute to the detected four-wave mixing signal. Only signals from interpulse mixing following $\omega_{\mathrm{FWM}}^{\text{non-degenerate}} = 2\omega_1 - \omega_2$ are observed with $\omega_2 > \omega_1$, where ω_1 and ω_2 are the central frequencies of the two pulses. In this case, eq 1 simplifies to

$$I(\omega_S) = c\varepsilon_0|\chi^{(3)} \int_{\omega_{\min}}^{\omega_{\max}} \mathrm{d}\Omega E_1^2(\Omega) \times E_2(2\Omega - \omega_S)e^{i[2\cdot\varphi(\Omega)-\varphi(2\cdot\Omega-\omega_S)]}|^2 \quad (2)$$

for the Stokes side. We find again a very good agreement between our parameter-free calculation and the experimental spectrum, assuming a spectrally constant $\chi^{(3)}$ response, as shown in Figure 1b.

Using either the low or the high energy side of the emission as a signal for an intensity map, we are able to detect high contrast confocal images of graphene as shown in Figure 1c. The signal on the detector reaches several million counts per second at a laser pulse energy of 5.4 pJ. Therefore, it is easily detected. In combination with the weak background stemming probably from the immersion oil and the glass substrate, near degenerate four-wave mixing provides a very clear contrast and high signal-to-noise ratio imaging.

Using amplitude pulse shaping we can readily verify the power dependence of the ND-FWM signal. For the Stokes side, the dependence on the input power is quadratic for $I_1 \propto |E_1|^2$ and linear for $I_2 \propto |E_2|^2$ and vice versa for the anti-Stokes side. The four resulting power laws are confirmed on single layer graphene as shown in Figure 2a.

Additionally, it is possible to verify the FWM origin of the signal within the probed range directly by scanning the frequency spacing between the central frequencies of the individual pulses using amplitude shaping (Figure 2b). The dependence of the input frequencies and of the input power as well as the good agreement with the theoretical curves for different spectral pulse shapes confirms that the detected signal stems mainly from FWM with a spectrally flat amplitude $\chi^{(3)}$ response.

A key requirement for broadband pulse characterization is a well-defined spectral phase response of the sample. In order to check for a phase dependence of the FWM signal in single layer graphene, we perform chirp scans. The linear chirp c (corresponding to a constant group delay dispersion) of a laser pulse is the second order polynomial spectral phase: $\phi(\omega) = \phi_0 + (c/2)(\omega_0 - \omega)^2$.[25] We apply a well-defined chirp to the pulse using a pulse shaper and monitor the corresponding ND-FWM signal on the Stokes and anti-Stokes side (for experimental details see Supporting Information). Our data

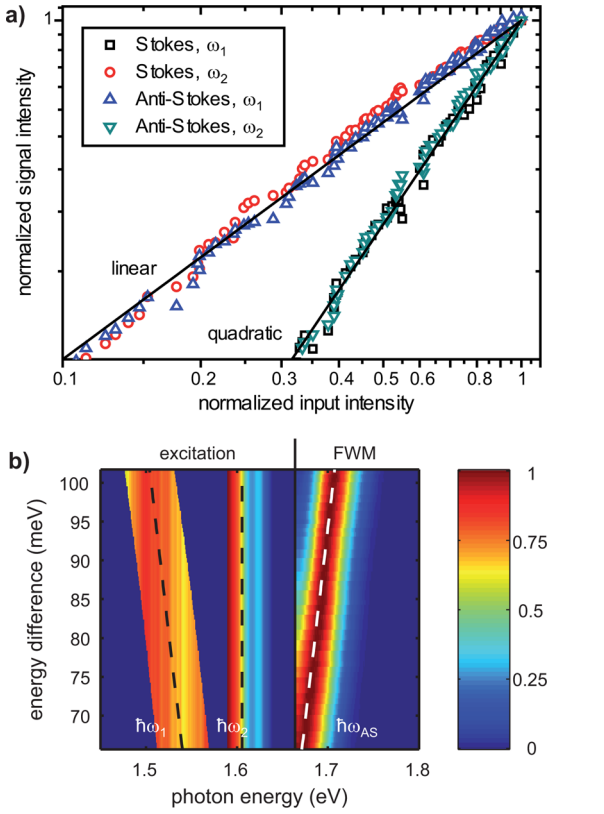

Figure 2. (a) Stokes and anti-Stokes power dependence of the FWM signal. Two narrow-band pulses are cut out of the full spectrum by the pulse shaper and individually varied in power. The measured power dependencies (symbols) match the theoretical curves (solid lines) in all four possible cases. (b) Control of FWM by scanning the energy difference between two pulses shifts the anti-Stokes band (Stokes not shown). FWM are normalized to one, ω_1 and ω_2 are the center-of-mass frequencies of the individual pulses, and the anti-Stokes frequency follows as $\omega_{AS} = 2\omega_2 - \omega_1$.

shows a strong dependence of the FWM signal on the applied chirp, Figure 3a.

This is expected since adding chirp to a femtosecond laser pulse leads to temporal broadening decreasing the maximum field intensity. Importantly, the maximum FWM signal occurs for zero chirp for all photon energies. A shift of the whole pattern along the chirp axis would indicate a second order

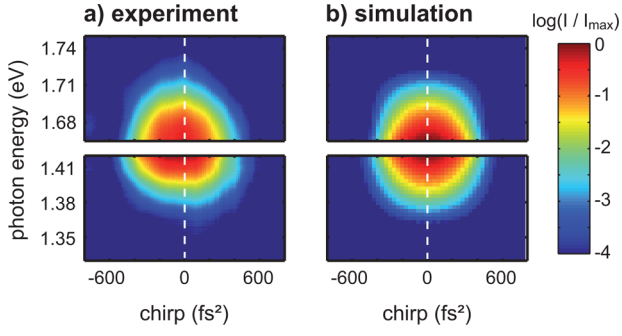

Figure 3. (a) Normalized SLG-FWM signal as a function of the chirp of the excitation laser pulse (logarithmic scale). The signal maximum is at 0 fs^2 indicating that the material itself produces the highest signal for a pulse with flat phase (input spectrum as in Figure 1a). (b) Simulation on the basis of a flat phase $\chi^{(3)}$ following eq 1.

DOI: 10.1021/acs.nanolett.5b00893
Nano Lett. 2015, 15, 4968−4972

phase dependence in $\chi^{(3)}$, as follows from eq 1. The same applies to higher even polynomial orders, while higher odd orders would result in a nonsymmetric shape of the pattern. We thus conclude that the chirp dependence is only due to the associated intensity variation and that the graphene phase response causes no additional chirp, i.e. is dispersionless in the probe spectral range. Figure 3b plots the theoretical ND-FWM signal according to eq 1. This agrees well with the experimental data in Figure 3a, corroborating the claim of a flat phase $\chi^{(3)}$.

We now demonstrate that due to its spectrally flat amplitude and phase, the strong near-degenerate four-wave mixing signal from graphene can be used for intrafocus phase characterization and compression of broadband pulses, assuming a uniform spatial beam profile. In this scheme, the ND-FWM signal for a laser pulse of unknown phase is maximized by varying the spectral phase profile of the pulse using a pulse shaper. In a first step, the ND-FWM signal is detected while scanning the second and third order of the phase (see Supporting Information Figure S4). The peak phase is then used as the starting point for the following procedure.

Final reconstruction of the phase or, more precisely, its second derivative, is achieved by maximizing the ND-FWM signal using a genetic algorithm.[31] The second order phase is varied at nine nodal points over the spectrum, while the parts in between are approximated by cubic interpolation. The number of parameters for the genetic algorithm is 9, allowing for a rapid convergence, typically within 10 to 20 generations. The actual phase applied to the pulse shaper is calculated by double integration with arbitrary integration constants. This can be done because the first (polynomial) order of the phase does not contribute to the pulse shape and the phase offset (carrier envelope phase) cannot be measured by a third order process, while having negligible influence for the shape of a 15 fs laser pulse.

After compressing the pulse by maximizing the ND-FWM signal, the result is compared to the procedure of multiphoton intrapulse interference phase scans (MIIPS[21]), using the second harmonic of iron(III) iodate nanocrystals detected in the same microscope. Figure 4b demonstrates a very small residual phase at the detection limit of the system. An interferometric second harmonic autocorrelation scan further verifies that the pulse is bandwidth limited after compression (Figure 4c). This demonstrates the feasibility of phase characterization using the near-degenerate four-wave mixing signal from single layer graphene.

We now compare our approach with current schemes and materials. From a materials perspective, graphene has several advantages. Its subnanometers thickness provides the optimum focus definition, which is particularly relevant for microscopy applications. In contrast, for other materials, such as beta barium borate nanocrystals, the size is typically on the order of several tens of nanometers, adding uncertainty to the focal position and depth. In the worst case, this could include propagation effects in the nonlinear response, causing erroneous phase corrections. We note that while two-dimensional graphene can be used to define the axial focus position very accurately, it does not provide information on the lateral focus properties. Beam distortions, such as a spatial chirp, can thus not be directly detected. Therefore, a clean laser mode is very important for the present measurement. In case of spatially distorted mode profiles, other techniques that are based on nanoscale probes, not directly relying on the mode profile, can be used (see for example, refs 22 and 32).

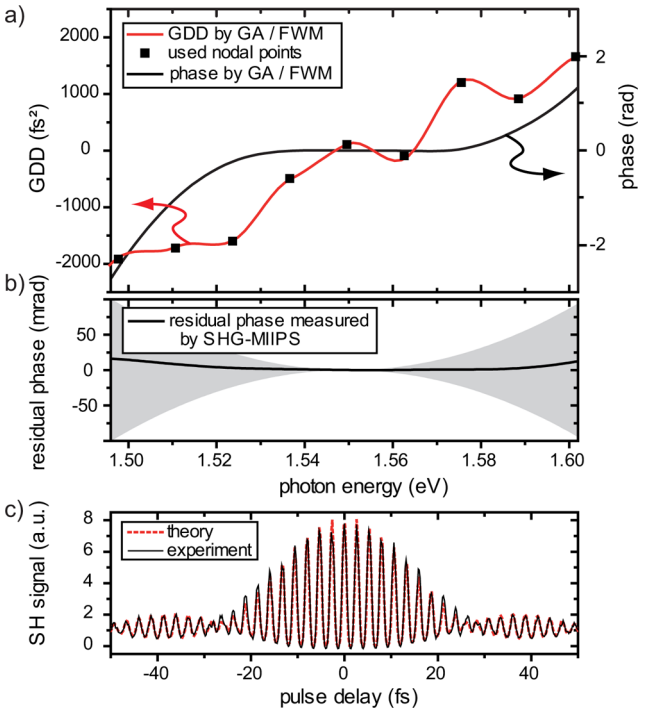

Figure 4. Demonstration of pulse compression using a genetic algorithm (GA) to maximize the ND-FWM signal on the anti-Stokes side of the laser. (a) Reconstructed group delay dispersion (GDD) of the pulse (red line), approximated by cubic interpolation between nine nodal points (black symbols), used as free parameters for the optimization. The shown spectral phase (black line) is the double integrated GDD with arbitrary integration constants. (b) Residual phase measured by MIIPS from second harmonic generation (SHG) on iron(III) iodate nanocrystals. The gray area is a conservative estimate of the error. (c) Second harmonic generation autocorrelation with the phase correction of panel a shows very good agreement with the theoretical curve obtained from the input spectrum.

At the same time, the graphene four-wave mixing is an extremely efficient process leading to easily detectable signals reaching photon count rates of several millions per second. Most importantly, its spectrally uniform response should allow for phase characterization of laser pulses reaching from the terahertz to the visible regime.

Near-degenerate FWM avoids drawbacks of schemes relying on higher harmonic detection and the associated requirements regarding the achromaticity and the large spectral detection range as discussed in the following. This could be particularly useful for pulses in the visible and for ultrabroadband pulses. Moreover, near-degenerate FWM at a given detection frequency contains the contribution of a broad range of input frequencies following eq 1. The ND-FWM signal is thus maximized if $\varphi(\Omega_1) + \varphi(\Omega_2) - \varphi(\Omega_1 + \Omega_2 - \omega) = 0$ for all combinations of Ω_1 and Ω_2. This can be achieved for a spectrally flat phase only. Therefore, in the limits of $\omega \approx \omega_{min}$ or $\omega \approx \omega_{max}$, all spectral components contribute. As a consequence, no spectrometer is required for pulse characterization when using a spectrally integrated signal sufficiently close to the excitation spectrum. The pulse optimization procedure could therefore be more robust compared to, for example, FROG or MIIPS, which require the detection of the full second harmonic spectrum.[20,21]

We note that, for ultrabroadband pulses exceeding 1600 cm^{-1} bandwidth, nonlinear Raman scattering from the G mode

DOI: 10.1021/acs.nanolett.5b00893
Nano Lett. 2015, 15, 4968−4972

in graphene could contribute to the detected signal. In this case, the procedure could be modified, for example, the spectrum could be compressed stepwise by limiting the bandwidth. We also note that other pulse characterization procedures based on FWM have been presented, for example, in combination with an additional gate pulse[33] or spectral detection analogous to FROG.[34] Compared to these procedures, the presented approach based on graphene's near-degenerate four-wave mixing appears to be simpler and more easily implemented. Very recently a femtosecond photocurrent response of graphene was demonstrated in ref 35 that can also be used for pulse measurements based on an electrical readout.

In summary, we showed that the near-degenerate four-wave mixing signal in single layer graphene can be described by a dispersionless and instantaneous $\chi^{(3)}$-process as expected from the linear band structure. The high and background free signal of several million counts per second makes ND-FWM ideal for nonlinear microscopy applications. Because there is no material specific phase influencing the signal, graphene proves to be uniquely suited for phase characterization of ultrafast pulses as demonstrated by compressing a 15 fs pulsed laser. This is of particular advantage for microscopy applications with broadband lasers or lasers in the visible, where second or third harmonic generation as a tool for pulse characterization is no longer feasible, because of the large spectral window that has to be covered by the optics.

■ ASSOCIATED CONTENT

Supporting Information

Experimental details about the pulse shaper, detection scheme, and sample material. The Supporting Information is available free of charge on the ACS Publications website at DOI: 10.1021/acs.nanolett.5b00893.

■ AUTHOR INFORMATION

Corresponding Author

*E-mail: achim.hartschuh@cup.uni-muenchen.de.

Notes

The authors declare no competing financial interest.

■ ACKNOWLEDGMENTS

We acknowledge support from the Deutsche Forschungsgemeinschaft through SPP 1391 (HA4405/6-1) and the Nanosystems Initiative Munich (NIM), the ERC starting Grant NEWNANOSPEC (279494), the synergy Grant Hetero2D, the EU Graphene Flagship (no. 604391), a Royal Society Wolfson Research Merit Award and the EPSRC Grants EP/K01711X/1, EP/K017144/1, and EP/L016087/1.

■ REFERENCES

(1) Geim, A. K.; Novoselov, K. S. *Nat. Mater.* **2007**, *6*, 183−191.
(2) Bonaccorso, F.; Sun, Z.; Hasan, T.; Ferrari, A. C. *Nat. Photonics* **2010**, *4*, 611.
(3) Koppens, F. H. L.; Mueller, T.; Avouris, P.; Ferrari, A. C.; Vitiello, M. S.; Polini, M. *Nat. Nanotechnol.* **2014**, *9*, 780.
(4) Ferrari, A. C.; Bonaccorso, F.; Falko, V.; Novoselov, K. S.; Roche, S.; Bøggild, P.; Borini, S.; Koppens, F.; Palermo, V.; Pugno, N. *Nanoscale* **2014**, *7*, 4587−5062.
(5) Xia, F.; Mueller, T.; Lin, Y.-M.; Valdes-Garcia, A.; Avouris, P. *Nat. Nanotechnol.* **2009**, *4*, 839−843.
(6) Vicarelli, L.; Vitiello, M. S.; Coquillat, D.; Lombardo, A.; Ferrari, A. C.; Knap, W.; Polini, M.; Pellegrini, V.; Tredicucci, A. *Nat. Mater.* **2012**, *11*, 865.
(7) Sun, Z.; Hasan, T.; Torrisi, F.; Popa, D.; Privitera, G.; Wang, F.; Bonaccorso, F.; Basko, D. M.; Ferrari, A. C. *ACS Nano* **2010**, *4*, 803−810.
(8) Lui, C. H.; Mak, K. F.; Shan, J.; Heinz, T. F. *Phys. Rev. Lett.* **2010**, *105*, 127404.
(9) Mikhailov, S. A. *EPL* **2007**, *79*, 27002.
(10) Hendry, E.; Hale, P. J.; Moger, J.; Savchenko, A. K.; Mikhailov, S. A. *Phys. Rev. Lett.* **2010**, *105*, 097401.
(11) Wu, R.; Zhang, Y.; Yan, S.; Bian, F.; Wang, W.; Bai, X.; Lu, X.; Zhao, J.; Wang, E. *Nano Lett.* **2011**, *11*, 5159−5164.
(12) Mikhailov, S. A. *Phys. E* **2012**, *44*, 924−927.
(13) Xenogiannopoulou, E.; Aloukos, P.; Couris, S.; Kaminska, E.; Piotrowska, A.; Dynowska, E. *Opt. Commun.* **2007**, *275*, 217.
(14) Luo, Z.; Zhou, M.; Wu, D.; Ye, C.; Weng, J.; Dong, J.; Xu, H.; Cai, Z.; Chen, L. *J. Lightwave Technol.* **2011**, *29*, 2732−2739.
(15) Xu, B.; Martinez, A.; Yamashita, S. *IEEE Photon. Technol. Lett.* **2012**, *24*, 1792−1794.
(16) Li, B.; Cheng, Y.; Liu, J.; Yi, C.; Brown, A. S.; Yuan, H.; Vo-Dinh, T.; Fischer, M. C.; Warren, W. S. *Nano Lett.* **2012**, *12*, 5936−5940.
(17) Pendry, J. B. *Science* **2008**, *322*, 71−73.
(18) Harutyunyan, H.; Beams, R.; Novotny, L. *Nat. Phys.* **2013**, *9*, 423−425.
(19) Lozovoy, V. V.; Dantus, A. M. *ChemPhysChem* **2005**, *6*, 1970.
(20) Trebino, R.; DeLong, K. W.; Fittinghoff, D. N.; Sweetser, J. N.; Krumbügel, M. A.; Richman, B. A.; Kane, D. J. *Rev. Sci. Instrum.* **1997**, *68*, 3277−3295.
(21) Lozovoy, V. V.; Pastirk, I.; Dantus, M. *Opt. Lett.* **2004**, *29*, 775−777.
(22) Accanto, N.; Nieder, J.-B.; Piatkowski, L.; Castro-Lopez, M.; Pastorelli, F.; Brinks, D.; van Hulst, N. *Light: Sci. Appl.* **2014**, *3*, e143.
(23) Comin, A.; Ciesielski, R.; Piredda, G.; Donkers, K.; Hartschuh, A. *J. Opt. Soc. Am. B* **2014**, *31*, 1118−1125.
(24) Bonacina, L.; Mugnier, Y.; Courvoisier, F.; Le Dantec, R.; Extermann, J.; Lambert, Y.; Boutou, V.; Galez, C.; Wolf, J. *Appl. Phys. B: Laser Opt.* **2007**, *87*, 399.
(25) Boyd, R. W. *Nonlinear Optics*, 3rd ed.; Academic Press: New York, 2003.
(26) Min, W.; Lu, S.; Rueckel, M.; Holtom, G. R.; Xie, X. S. *Nano Lett.* **2009**, *9*, 2423.
(27) Because of the tight focusing of fields and the resulting spatially nonuniform intensity, nonlinear material constants are difficult to quantify in microscopic measurements. The reported value for $\chi^{(3)}$ represents the equivalent obtained for plane wave excitation with a circular diameter of 375 nm. While the individual characteristics of the components in the detection beam path are well-known, such as filter transmission and camera sensitivity, they add up to a total uncertainty of about an order of magnitude.
(28) Mikhailov, S. A. *Phys. Rev. B: Condens. Matter Mater. Phys.* **2014**, *90*, 241301.
(29) Stöhr, R. J.; Kolesov, R.; Pflaum, J.; Wrachtrup, J. *Phys. Rev. B: Condens. Matter Mater. Phys.* **2010**, *82*, 121408.
(30) Winzer, T.; Ciesielski, R.; Handloser, M.; Comin, A.; Hartschuh, A.; Malic, E. *Nano Lett.* **2015**, *15*, 1141−1145.
(31) Mathworks Inc., Genetic Algorithm Solver of the Global Optimization Toolbox 2009; tp://uk.mathworks.com/products/global-optimization/features.html#genetic-algorithm-solver (accessed July 1, 2015).
(32) Pawłowska, M.; Goetz, S.; Dreher, C.; Wurdack, M.; Krauss, E.; Razinskas, G.; Geisler, P.; Hecht, B.; Brixner, T. *Opt. Express* **2014**, *22*, 31496.
(33) Selm, R.; Krauss, G.; Leitenstorfer, A.; Zumbusch, A. *Opt. Express* **2012**, *20*, 5955.
(34) Petrillo, K. G.; Wang, K.-Y.; Foster, A. C.; Foster, M. A. *Opt. Express* **2013**, *21*, 31229.
(35) Tielrooij, K. J.; Piatkowski, L.; Massicotte, M.; Woessner, A.; Ma, Q.; Lee, Y.; Myhro, K. S.; Lau, C. N.; Jarillo-Herrero, P.; van Hulst, N.; Koppens, F. H. L. *Nat. Nanotechnol.* **2015**, *10*, 437.

DOI: 10.1021/acs.nanolett.5b00893
Nano Lett. 2015, 15, 4968−4972